High-resolution measurements of near-edge resonances in the core-level photoionization spectra of SF_6

E. Hudson and D. A. Shirley*
Department of Chemistry, University of California, Berkeley, California 94720
and Chemical Sciences Division, MS 2-300, Lawrence Berkeley Laboratory, 1 Cyclotron Road, Berkeley, California 94720

M. Domke, G. Remmers, A. Puschmann, T. Mandel, and C. Xue
Institut für Experimentalphysik, Freie Universität Berlin, Arnimallee 14, W-1000 Berlin 33, Germany

G. Kaindl
Institut für Experimentalphysik, Freie Universität Berlin, Arnimallee 14, W-1000 Berlin 33, Germany
and Chemical Sciences Division, MS 2-300, Lawrence Berkeley Laboratory, 1 Cyclotron Road, Berkeley, California 94720
(Received 26 March 1992; revised manuscript received 31 August 1992)

The x-ray-absorption near-edge structure (XANES) of sulfur hexafluoride, SF_6, in the gas phase has been measured with high energy resolution at the sulfur $L_{2,3}$ and fluorine K ionization thresholds using synchrotron radiation from the SX700/II monochromator at BESSY. Besides dominant transitions to core-excited inner-well states, several series of Rydberg states with vibrational fine structure were resolved below the sulfur $L_{2,3}$ thresholds. Using the Rydberg formula, quantum defects of $\delta_s = 1.80$ and $\delta_d = -0.03$ were obtained for the s and d Rydberg orbitals of the central sulfur atom. A Franck-Condon analysis was used to determine the vibrational spacing and the S—F bond length of the $(S\ 2p_{3/2})^{-1}4s^1$ core-excited state. The presence of vibronically coupled transitions below the sulfur $L_{2,3}$ edges was confirmed. The derived natural linewidths of the $(S\ 2p_{1/2,3/2})^{-1}$ Rydberg states were found to be strikingly narrower than those of the $(S\ 2p_{1/2,3/2})^{-1}$ inner-well resonances. Line-shape analysis also revealed significant inhomogeneous broadening of the $(S\ 2p_{1/2,3/2})^{-1}a_{1g}^1$ states, which is attributed to unresolved vibrational structure. Large Lorentzian contributions to the line shapes of the $(S\ 2p_{1/2,3/2})^{-1}t_{2g}^1$ resonances suggest that vibrational effects are relatively small for those states.

PACS number(s): 33.20.Rm, 33.70.−w, 33.80.Eh, 33.80.Rv

I. INTRODUCTION

Recent advances in soft-x-ray monochromators at synchrotron radiation facilities allow unprecedented combinations of spectral resolution and photon flux. Several monochromators now have resolving powers on the order of 10^4 at the nitrogen K edge [1–4], facilitating the measurement of high-resolution x-ray-absorption near-edge structure (XANES) in atoms and molecules [5,6]. Photoabsorption spectra exhibit fine structure both above and below core-level absorption edges. Some pre-edge resonances in molecules display very narrow natural linewidths and/or closely spaced vibrational states. In past years such structure was successfully measured at high resolution by electron-energy-loss spectroscopy (EELS) [7]. Although new developments in soft x-ray monochromators may not improve upon the resolution of EELS measurements, the inherent spectral brightness of synchrotron radiation allows the rapid collection of data with good signal-to-noise ratios.

Resonances in XANES spectra arise from the promotion of a core electron into a virtual orbital. The final state of the system is commonly described by referring to the character of the newly occupied orbital. In particular, the transition may be to an inner- or outer-well state. This scheme refers to the atomic partial-wave potential-energy diagram for an electron of angular momentum $l > 0$ (Fig. 1). The centrifugal contribution to the potential energy may combine with the electrostatic contributions to produce a potential barrier as shown. In molecules the electrons around the outer atoms produce a similar barrier along the bond directions. Virtual orbitals with a spatial distribution primarily inside the potential barrier are known as inner-well orbitals. If an electron is promoted into such a valence orbital, the system is said to be in an inner-well state. Allowed transitions to these states are normally quite intense in XANES spectra. If the virtual orbital is located mainly in the outer well, the transition is to a Rydberg state. These transitions are normally weak in XANES spectra as a result of poor spatial overlap between the initial- and final-state orbitals. Transitions to bound inner-well states lie at energies below transitions to Rydberg states. The Rydberg resonances have a series of energies which converge on the absorption edge from below. Transitions to quasibound inner-well states are referred to as shape resonances and occur at energies above the absorption edge.

This paper presents measurements of the XANES of gaseous SF_6 at the sulfur $L_{2,3}$ and fluorine K edges. Previous photoabsorption [8–14] and EELS [15] measurements showed intense resonances both above and below these thresholds, arising from the promotion of a core

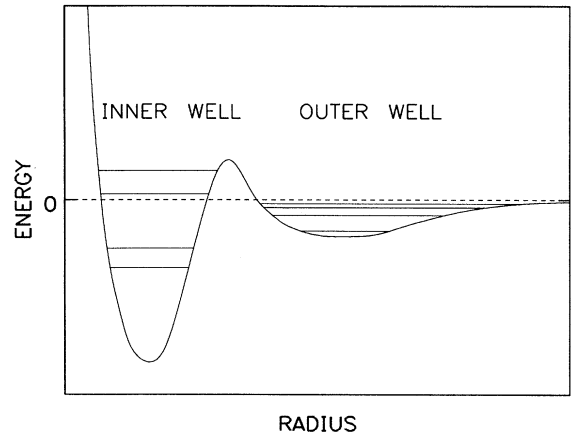

FIG. 1. Schematic representation of a double-well potential (not to scale). The barrier divides the potential curve into two regions, the inner well and the outer well. Valence orbitals are located mainly in the inner well. Rydberg orbitals are located mainly in the outer well. Some possible energies of such orbitals are shown as horizontal lines in the figure. Note that in some inner-well states the electron has positive energy. Such states are quasibound; the electron rapidly tunnels through the barrier and escapes the molecule.

electron into a virtual molecular orbital with large amplitude within the molecule. Very weak Rydberg resonances were also detected just below the sulfur $L_{2,3}$ edges, but were not completely characterized. In the present work, improved resolution and statistics resulted in the detection of weaker members of the Rydberg series below the sulfur $L_{2,3}$ edges. This allows an unambiguous assignment of peaks in this region, including the confirmation of vibronically coupled excitations. Quantum defects, spin-orbit splitting, and the $L_{2,3}$ absorption-threshold energies were determined from a least-squares fit of the spectrum. Vibrational structure was resolved for the first time in several Rydberg states. A Franck-Condon analysis yielded the vibrational spacing and S—F bond length for the core-excited $(S\ 2p_{3/2})^{-1}4s^1$ state. Multiplet splitting was observed for the $(S\ 2p_{1/2,3/2})^{-1}3d^1$ states. The derived natural linewidths of the $(S\ 2p_{3/2})^{-1}3d\text{-}t_{2g}^1$, $(S\ 2p_{3/2})^{-1}5s^1$, and $(S\ 2p_{3/2})^{-1}4d^1$ Rydberg states were found to be strikingly narrower than those of the $(S\ 2p_{1/2,3/2})^{-1}a_{1g}^1$ inner-well resonances. High signal-to-noise ratios in the spectra of the more intense resonances allowed line-shape analyses. Inhomogeneous broadening of the $(S\ 2p_{1/2,3/2})^{-1}a_{1g}^1$ states is attributed to unresolved vibrational structure. The peaks assigned to the $(S\ 2p_{1/2,3/2})^{-1}t_{2g}^1$ states have large Lorentzian components, suggesting that vibrational effects are relatively small for these shape resonances. Significant intensity very close in energy to the fluorine K edge could not be fitted by a simple edge-jump model and was assigned to a manifold of unresolved resonances. A previously unobserved resonance of large width and low intensity was detected above both the sulfur $L_{2,3}$ and fluorine K edges.

Section II of this paper gives experimental details of the measurements and details of the data analysis. Section III presents the measured spectra and peak assignments. These assignments and the results of curve fitting are discussed in detail in Sec. IV. The results are also compared to theoretical predictions in Sec. IV.

II. EXPERIMENT

Photoabsorption spectra were measured using soft x rays from the SX700/II monochromator of the Freie Universität Berlin at the Berliner Elektronenspeicherring für Synchrotronstrahlung (BESSY) [1,2,16]. A 1221-line/mm grating was employed for all measurements, except as noted below. Using this grating, some spectra were recorded using special low-emittance storage-ring conditions (small-source mode) to allow better resolution [1,2]. With normal emittance at BESSY, resolution in the first order of diffraction is $\approx$45 meV [Gaussian full width at half maximum (FWHM)] at the sulfur $L_{2,3}$ edges and $\approx$310 meV at the fluorine K edge. In the small-source mode, the resolution improves to $\approx$30 meV at the sulfur $L_{2,3}$ edges. Additional measurements were made using a 2442-line/mm grating in the first order of diffraction with normal emittance conditions, providing a resolution of $\approx$40 meV at the sulfur $L_{2,3}$ edges.

The synchrotron radiation beam passed through a 1500-Å-thick Al (1 at. % Si) window into an interaction region containing SF_6 gas. The absorption of radiation by the gas was measured by monitoring the total photoionization current in a photoabsorption cell with a 10-cm active length. The SF_6 gas (Messer Griesheim GmbH, 99.9%) was maintained at pressures ranging from 60 to 175 mTorr. For the measurements with the 2442-line/mm grating, a 1200-Å carbon window was used.

The spectra were analyzed using a least-squares curve-fitting routine. In regions of overlapping peaks, it was possible to deconvolute the individual contributions to the overall line shape. Each individual peak was modeled by a Voigt function, i.e., by a Lorentzian function convoluted with a Gaussian function. The Lorentzian (natural) linewidth corresponds to the lifetime broadening of the state. One contribution to the Gaussian linewidth stems from instrumental broadening due to the finite resolution of the monochromator. The resolution function is only approximated by a Gaussian line shape [1], but deviations from this approximation should not significantly affect the conclusions of the present work. A Gaussian line shape is also often used to approximate inhomogeneous broadening. In general, the total Gaussian linewidth derived from a fit will reflect both of these contributions. Further details of the data analysis are discussed in Sec. IV.

III. RESULTS

Figure 2 shows the photoabsorption spectrum of the octahedral molecule SF_6 across the sulfur $L_{2,3}$ edges. The double-peaked structure 1,2 at 172–174 eV arises from the promotion of a sulfur $2p$ electron to an unoccupied molecular orbital of a_{1g} symmetry. This absorption feature is split by the spin-orbit interaction of the $2p$ core

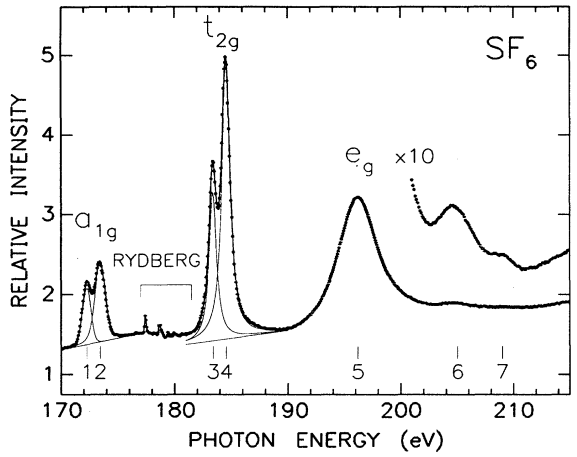

FIG. 2. Photoabsorption spectrum of SF_6 near the sulfur $L_{2,3}$ edges. The numbered peaks are assigned in Table I. For peaks 1–4, the line through the data points is a least-squares fit resulting in the individual components shown. Each component peak is a Voigt function. The results of the fit are given in Table I. The data points are connected in the Rydberg region to guide the eye. The inset data showing peaks 6 and 7 in greater detail were measured using the 2442-line/mm grating.

electrons in the final state. A more intense doublet 3,4 appears at 182–184 eV, just above the sulfur $L_{2,3}$ thresholds. It is assigned to the promotion of a single sulfur $2p$ electron to a quasibound orbital of t_{2g} symmetry, with spin-orbit splitting again accounting for the double-peaked structure. This is a well-known example of a molecular shape resonance, i.e., the promotion of an electron into a one-electron continuum state which is resonantly enhanced within the molecule by the molecular potential [17,18]. The broad absorption peak 5 at 196 eV is assigned to the excitation of a resonance of e_g symmetry. This state is a shape resonance which may couple to several other continuum channels and may also include contributions from autoionizing multielectron excitations [19]. The small peak 6 at 205 eV has been described as a multielectron excitation, but it is not yet fully understood [15]. An even smaller resonance, peak 7 at 209 eV, which appears to be doublet, is observed here for the first time and may also be a multielectron excitation. Note that the inset data of Fig. 2 showing peaks 6 and 7 in greater detail were taken using the 2442-line/mm grating. The known complexity of the e_g resonance suggests that the t_{2g} resonance may also be more than a simple one-electron excitation shape resonance. An autoionizing state with two excited electrons has been predicted near the energy of the t_{2g} resonance [19]. Another t_{2g} resonance of this molecule is known to couple to several continuum channels upon excitation at 23-eV photon energy [20]. A similar process is possible at the $L_{2,3}$ edges, as discussed below.

Figure 3 shows the spectrum in the 177–182-eV range obtained with better resolution and statistics using the 2442-line/mm grating. The weak fine structure detected in the spectrum of Fig. 2 is clearly resolved here. Many peaks are present: most are readily assigned to one-electron excitations into Rydberg orbitals. These Rydberg states correspond to those of atomic sulfur, the central atom, and will be labeled as such. The s- and d-symmetry Rydberg states form two overlapping series, each of which is split into two series by the spin-orbit interaction of the core hole. The resulting four series overlap to give the complicated structure observed. Such an assignment leaves the features E, F, and G around 178.2 eV unexplained. They are assigned to a vibronically coupled transition to the $(\mathrm{S}\ 2p_{3/2})^{-1}\ 4p'$ Rydberg state. In addition, the region from 177 to 179 eV is characterized by some broad intensity above background (shaded area), which is attributed to a vibronically coupled transition to a virtual orbital with t_{1u} symmetry.

Figure 4 shows the photoabsorption spectrum of SF_6 across the fluorine K edge. Peak 8 at 689.0 eV is assigned to a transition to the a_{1g} unoccupied molecular orbital, as seen at the sulfur $L_{2,3}$ edges. The following peaks 9, 10, and 11, below and just above the edge jump at 695.7 eV, are assigned to transitions to a number of t_{1u} virtual orbitals. Peaks 12 and 13, at 699.9 and 713.3 eV, are excitations to t_{2g} and e_g shape resonances, respectively, which are analogous to those seen at the sulfur $L_{2,3}$ edges. Peaks 14 and 15, at 722 and 727 eV, are probably multielectron excitations analogous to peaks 6 and 7 in Fig. 1. Note that transitions into orbitals of both g and u parity are observed here, arising from the combination of the six fluorine $1s$ atomic orbitals into the $2a_{1g}$, $1e_g$, and $1t_{1u}$ molecular orbitals of the initial state. Figure 5 shows a level diagram of the core-excited states of SF_6 based upon the energies and assignments given above and in Tables I–III.

TABLE I. SF_6 sulfur $2p$ inner-well resonances: Assignments and fit results.

Peak	Energy (eV)	Assignment	Intensity (arb. units)	Width (FWHM, eV)
1	172.27	$a^1_{1g}\ (\mathrm{S}\ 2p_{3/2})^{-1}$	1.00	0.87
2	173.44	$a^1_{1g}\ (\mathrm{S}\ 2p_{1/2})^{-1}$	1.62	1.06
3	183.40	$t^1_{2g}\ (\mathrm{S}\ 2p_{3/2})^{-1}$	2.71	0.76
4	184.57	$t^1_{2g}\ (\mathrm{S}\ 2p_{1/2})^{-1}$	5.53	0.85
5	196.2	$e^1_g\ (\mathrm{S}\ 2p_{1/2,3/2})^{-1}$	15.7	4.1
6	205	multielectron excitation?		
7	209	multielectron excitation?		

IV. DISCUSSION

A. Sulfur $L_{2,3}$ thresholds: Inner-well resonances

1. Spin-orbit interaction and exchange interaction

Nearly all features observed near the sulfur $L_{2,3}$ thresholds clearly display a doublet structure, with a splitting of ≈ 1.2 eV. This can be explained by the spin-orbit interaction of the core electrons in the final state. According to Hund's rule, the $(S\ 2p_{1/2})^{-1}$ configuration will have higher energy than the $(S\ 2p_{3/2})^{-1}$ configuration. The value of the splitting observed here agrees with the measured splittings in x-ray photoelectron spectra (XPS) of SF_6 [21]. The multiplicities of the $(S\ 2p_{1/2})^{-1}$ and $(S\ 2p_{3/2})^{-1}$ configurations are 2 and 4, respectively. A statistical model of the core-excited final state would predict a doublet with a peak intensity ratio $(S\ 2p_{3/2})^{-1}$:$(S\ 2p_{1/2})^{-1}$ of 2:1. This ratio was observed in the XPS spectrum [22], but is not observed for the $(S\ 2p_{1/2,3/2})^{-1}a_{1g}^1$ and $(S\ 2p_{1/2,3/2})^{-1}t_{2g}^1$ photoabsorption resonances. In fact, the ratios for these resonances, obtained from least-squares fits of the spectrum in Fig. 2, are both less than unity (see Table I).

This reversal of the intensity ratio can be explained by including the effects of exchange interaction between the core hole and the excited electron [17,23]. The $(S\ 2p_{1/2,3/2})^{-1}a_{1g}^1$ and $(S\ 2p_{1/2,3/2})^{-1}t_{2g}^1$ resonances (peaks

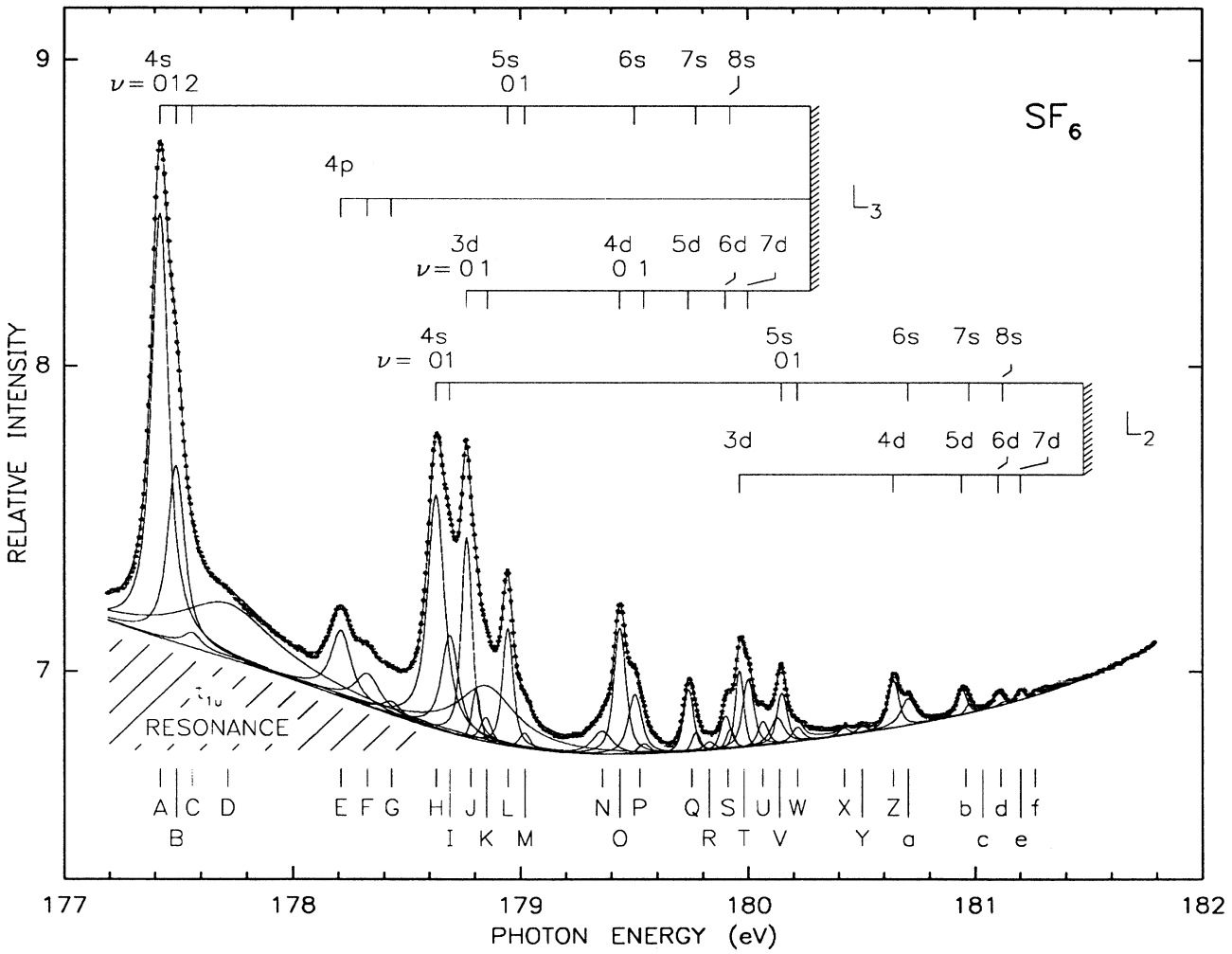

FIG. 3. Sulfur $L_{2,3}$ pre-edge fine structure of the SF_6 photoabsorption spectrum. The shaded area indicates the contribution of the $(S\ 2p_{1/2,3/2})^{-1}t_{1u}^1$ transitions to the overall background. The peaks labeled by letters are assigned in Table II. The line through the data points is the result of a least-squares fit. For the fit, the background was modeled by a linear contribution, the tail of a Voigt function from peak 3 (see Fig. 2), and several overlapping Gaussian peaks to represent the $(S\ 2p_{1/2,3/2})^{-1}t_{1u}^1$ transitions. Each of the individual component peaks shown is a Voigt function. The results of the fit are given in Table II. The data in this figure were measured using the 2442-line/mm grating.

TABLE II. SF_6 sulfur $2p$ Rydberg states: Assignments and fit results.

Peak	Energy (eV)	Assignment	Intensity (arb. units)	Width (FWHM, meV)
A	177.42	$4s^1$ (S $2p_{3/2})^{-1}$	100.0	76
B	177.49	vibration	41.7	76
C	177.56	vibration		
D	177.72	background		
E	178.21	$4p^1$ (S $2p_{3/2})^{-1}$	19.4	102
F	178.33	vibration		
G	178.43	vibration		
H	178.63	$4s^1$ (S $2p_{1/2})^{-1}$	54.7	85
I	178.69	vibration		
J	178.76	$3d\text{-}t_{2g}^1$ (S $2p_{3/2})^{-1}$	27.2	57
	178.80	$3d\text{-}e_g^1$ (S $2p_{3/2})^{-1}$		
K	178.85	vibration ($3d\text{-}t_{2g}$)		
	178.85	background		
L	178.95	$5s^1$ (S $2p_{3/2})^{-1}$	15.4	54
M	179.02	vibration		
N	179.36	$4p^1$ (S $2p_{1/2})^{-1}$		
O	179.44	$4d^1$ (S $2p_{3/2})^{-1}$	19.1	60
P	179.50	$6s^1$ (S $2p_{3/2})^{-1}$	10.6	67
	179.54	vibration ($4d$)		
Q	179.74	$5d^1$ (S $2p_{3/2})^{-1}$		
	179.77	$7s^1$ (S $2p_{3/2})^{-1}$		
R	179.83	vibration ($5d$)		
S	179.90	$6d^1$ (S $2p_{3/2})^{-1}$		
	179.92	$8s^1$ (S $2p_{3/2})^{-1}$		
T	179.96	$3d\text{-}t_{2g}^1$ (S $2p_{1/2})^{-1}$		
	180.00	$7d^1$ (S $2p_{3/2})^{-1}$		
	180.00	$3d\text{-}e_g^1$ (S $2p_{1/2})^{-1}$		
U	180.05	vibration ($3d\text{-}t_{2g}$)		
	180.06	$8d^1$ (S $2p_{3/2})^{-1}$		
V	180.13	$9,10d^1$ (S $2p_{3/2})^{-1}$		
	180.15	$5s^1$ (S $2p_{1/2})^{-1}$		
W	180.22	vibration		
L_3 edge	180.27			
X	180.42	$5p^1$ (S $2p_{1/2})^{-1}$		
Y	180.50	vibration		
Z	180.64	$4d^1$ (S $2p_{1/2})^{-1}$		
a	180.71	$6s^1$ (S $2p_{1/2})^{-1}$		
b	180.94	$5d^1$ (S $2p_{1/2})^{-1}$		
	180.97	$7s^1$ (S $2p_{1/2})^{-1}$		
c	181.03	vibration ($5d$)		
d	181.10	$6d^1$ (S $2p_{1/2})^{-1}$		
	181.12	$8s^1$ (S $2p_{1/2})^{-1}$		
e	181.20	$7d^1$ (S $2p_{1/2})^{-1}$		
f	181.27	$8d^1$ (S $2p_{1/2})^{-1}$		
L_2 edge	181.48			

TABLE III. SF_6 fluroine K inner-well resonances: Assignments and fit results.

Peak	Energy (eV)	Assignment	Intensity (arb. units)	Width (FWHM, eV)
8	689.0	a_{1g}^1 (F $1s)^{-1}$	1.000	2.2
9	692.9	t_{1u}^1 (F $1s)^{-1}$	0.448	2.1
10	694.7	t_{1u}^1 (F $1s)^{-1}$	0.672	2.1
11	696.3	t_{1u}^1 (F $1s)^{-1}$	0.338	3.1
12	699.9	t_{2g}^1 (F $1s)^{-1}$	0.644	2.2
13	713.2	e_g^1 (F $1s)^{-1}$	0.96	4.6
14	722	mutlielectron excitation?		
15	727	multielectron excitation?		

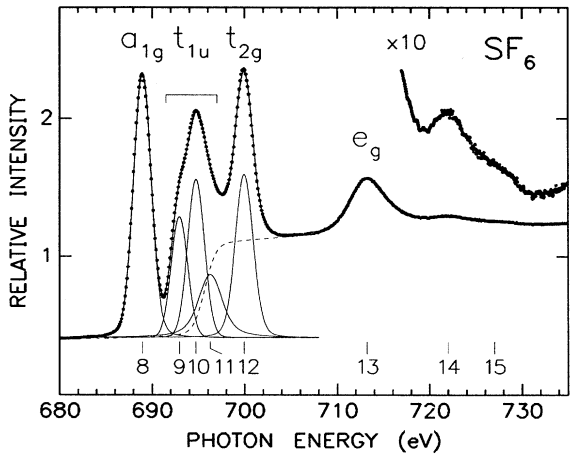

FIG. 4. Photoabsorption spectrum of SF_6 near the fluorine K edge. The numbered peaks are assigned in Table III. The line through the data points from 680 to 708 eV is a least-squares fit with the individual components shown. Each component peak is a Voigt function. A Gaussian-broadened arctangent function models the edge jump. The results of the fit are given in Table III.

2,1 and 4,3, respectively) arise from one-electron transitions into unoccupied molecular orbitals spatially localized within the molecule. An electron excited from a core hole into such an inner-well state will have strong overlap with the remaining sulfur core electrons. The resulting core-hole–excited-electron exchange interaction will be significant in comparison to the spin-orbit interaction. In such a case the j-j coupling scheme used above is no longer valid; intermediate coupling must be employed. Theoretical studies of this phenomenon in SF_6 and other systems show that the main effect of intermediate coupling is to decrease the $(S\ 2p_{3/2})^{-1}$ to $(S\ 2p_{1/2})^{-1}$ intensity ratio [24]. In the limit where exchange coupling completely dominates over spin-orbit coupling, the intensity ratio becomes zero because the lower-energy peak then represents a dipole-forbidden transition into a triplet state. Calculations also predict that intermediate coupling has little effect on the energy splitting of the doublet [24], in agreement with the present observations (see Tables I and II). The spin-orbit splittings of the $(S\ 2p_{1/2,3/2})^{-1}a_{1g}^1$ and $(S\ 2p_{1/2,3/2})^{-1}t_{2g}^1$ doublets (1.17 eV) are only $\approx 3\%$ less than those of the Rydberg states (1.20 eV), where the exchange interaction is expected to be small because of the limited overlap of the Rydberg orbitals with the core hole.

2. *Line shapes*

Attempts to fit the $(S\ 2p_{1/2,3/2})^{-1}a_{1g}^1$ resonance doublet (peaks 1,2) with a pair of Voigt functions based on reasonable values of the Lorentzian natural linewidth and the Gaussian instrumental width were unsuccessful. The a_{1g} resonance therefore appears to be inhomogeneously broadened. This probably arises from extensive vibrational excitations in the final state, resulting in an overlapping manifold of peaks. Such excitations are expected, because a nonbonding core electron has been promoted into an antibonding orbital. Semiempirical calculations [25] for the ground state of the octahedral molecule ClF_6, which is the equivalent-core molecule to S-core-excited SF_6, predict a bond length of 1.63 Å for Cl—F [equivalent to S—F in the core-excited $(S\ 2p_{1/2,3/2})^{-1}a_{1g}^1$ state of SF_6] compared to 1.561 Å in ground-state SF_6 [26]. Such a large change in bond length would produce the extensive vibrational excitation suggested here. The only dipole-allowed vibrational excitation is the single a_{1g}

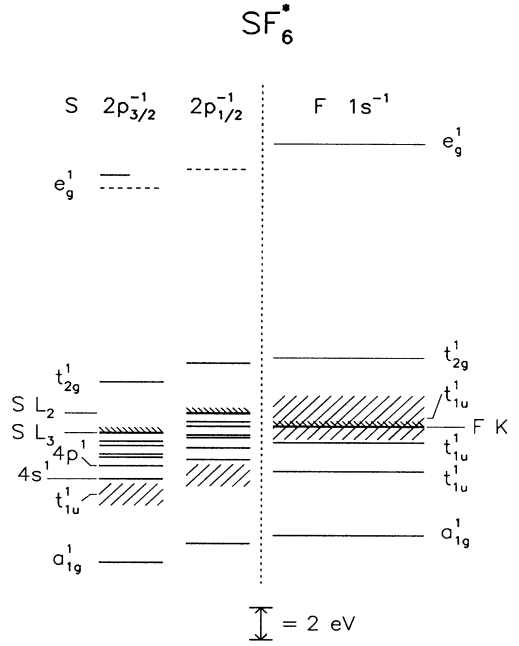

FIG. 5. Level diagram of the core-excited states of SF_6 at the sulfur $L_{2,3}$ and fluorine K edges. The relative energies of the states are plotted to scale, using the results given in Tables I–III. The fluorine K edge is aligned with the weighted average of the sulfur $L_{2,3}$ edges to facilitate the comparison of relative state energies. On the left side of the diagram, only the states with a $(S\ 2p_{3/2})^{-1}$ core hole are labeled. The corresponding states with a $(S\ 2p_{1/2})^{-1}$ core hole are shown as a separate series, but not labeled. Several Rydberg states are shown below the sulfur $L_{2,3}$ edges, but only the two lowest states are labeled. The spin-orbit splitting of the $(S\ 2p_{1/2,3/2})^{-1}e_g^1$ doublet was not resolved in the spectrum and the short solid horizontal line shows the energy of the single feature observed. The energies of these two individual states have been approximated by using the spin-orbit splitting and peak intensity ratio measured for the $(S\ 2p_{1/2,3/2})^{-1}t_{2g}^1$ doublet. The levels obtained are shown by the horizontal dashed lines. The shaded regions indicate the positions of broad features in the spectra which may include contributions from more than one state. In the case of the $(S\ 2p_{1/2,3/2})^{-1}t_{1u}^1$ shaded regions, the spin-orbit splitting shown was not actually resolved in the spectra, and, in addition, there may be two separate resonances. The broad shaded region at the fluorine K edge is tentatively assigned to an unresolved manifold of $(F\ 1s)^{-1}t_{1u}^1$ states. See text for further details.

symmetric-stretch mode, ν_1, (with ground-state frequency 774 cm^{-1}, corresponding to 96 meV) [27]. Measurements with very high resolution might resolve individual vibrational states, but no fine structure was observed in this study, even in the spectra taken in the small-source mode of BESSY with a resolution of ≈ 30 meV (spectrum not shown). This is presumably a consequence of the large natural linewidths of the individual vibrational states (determined to be > 220 meV, FWHM).

A Franck-Condon analysis [28] of the line shape of doublet 1,2 was performed, based on harmonic-oscillator potentials and Voigt line shapes. A good fit to the line shape was obtained only by using an excited-state vibrational spacing greater than that of the ground state ($h\nu_e \approx 125$ meV versus $h\nu_g = 96$ meV). The derived bond length ($R_e \approx 1.62$ Å) was close to the prediction from the equivalent-core molecule ClF_6, but an increase in bond length accompanied by an *increase* in the associated vibrational stretch frequency is difficult to explain. In the harmonic-oscillator approximation used here, equal contractions and extensions of the bond have equivalent effects on the Franck-Condon profile of transitions originating in the ground vibrational state. Thus the fit is also consistent with a decrease in the bond length ($R_e \approx 1.50$ Å), which, however, is hard to reconcile with the calculated bond length for ClF_6. Further studies are necessary to gain a better understanding of this excited state.

The total width of the (S $2p_{1/2})^{-1}a_{1g}^1$ peak is $\approx 20\%$ larger than that of the (S $2p_{3/2})^{-1}a_{1g}^1$ peak (see Table I). The shapes of the Franck-Condon envelopes for the two resonances should be identical, except for the effect of the natural linewidths of the individual vibrational states and a very small difference from the fourth-power dependence of the Franck-Condon factors on excitation energy. The natural linewidths resulting from the best fit based on this assumption ($\Gamma[(S\ 2p_{3/2})^{-1}a_{1g}^1] \approx 300$ meV (FWHM), $\Gamma[(S\ 2p_{1/2})^{-1}a_{1g}^1] \approx 400$ meV) are both quite large, especially in comparison with the exceptionally narrow natural linewidths (e.g., 24 meV) measured in the Rydberg region of this spectrum (see Sec. IV B 3). The large difference between the derived natural linewidths of the (S $2p_{1/2})^{-1}a_{1g}^1$ and (S $2p_{3/2})^{-1}a_{1g}^1$ states indicates different decay rates of the two excited states. The (S $2p_{1/2})^{-1}a_{1g}^1$ resonance may autoionize faster because it has more decay channels, perhaps including decay through the (S $2p_{3/2})^{-1}a_{1g}^1$ resonance. An analogous difference in linewidths has not been observed in the XANES spectra of rare gases (see, e.g., Ref. [1], Figs. 3–5). In these atomic systems, however, there are no vibrational or rotational levels to take up excess electronic energy, so that an inter-system crossing between nondegenerate electronic states is not possible. This effect might also be a further manifestation of intermediate coupling. Specifically the (S $2_{3/2})^{-1}a_{1g}^1$ state acquires some triplet-state character through exchange interaction. In the triplet state, the excited electron has its spin parallel to the unpaired sulfur $2p$ electron. The excited electron will avoid the unpaired electron and thus also avoid the core hole (which has the same spatial distribution). The result is a reduced probability for an autoionization process involving the excited electron (which may be the dominant decay process; see Sec. IV B 3). The (S $2p_{3/2})^{-1}a_{1g}^1$ peak narrows to reflect the increased lifetime of this state. The (S $2p_{1/2})^{-1}a_{1g}^1$ state has no triplet character and thus has a shorter lifetime. This explanation is consistent with the absence of the described effect in the XANES spectra of rare gases [1], since those systems do not exhibit intermediate coupling.

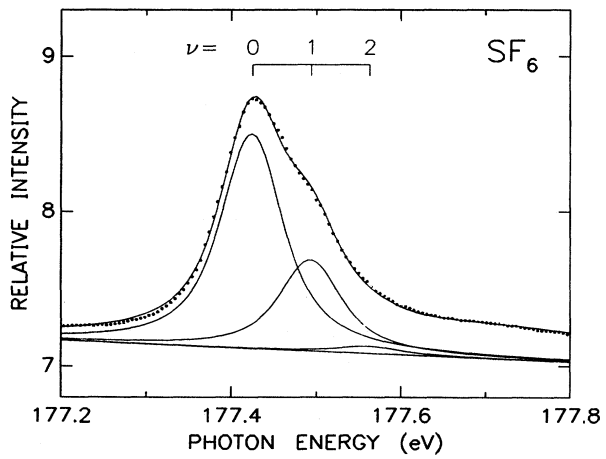

FIG. 6. Franck-Condon analysis of the vibrational structure of the (S $2p_{3/2})^{-1}4s^1$ state (peaks *A*, *B*, *C* in Fig. 3). The ground-state parameters were taken from Refs. [19] and [20] and the final-state parameters were varied to obtain the best fit. Each of the individual component peaks shown is a Voigt function. See text for further details.

A least-squares fit of the line shapes of the (S $2p_{3/2,1/2})^{-1}t_{2g}^1$ resonances (peaks, 3,4) using Voigt functions showed significant Lorentzian contributions. A good fit to the data was obtained using a single Gaussian width of 270 meV (FWHM) and Lorentzian widths of 690 and 783 meV for the (S $2p_{3/2})^{-1}t_{2g}^1$ and (S $2p_{1/2})^{-1}t_{2g}^1$ states, respectively. The bandwidth of radiation contributes ≈ 45 meV to the Gaussian width, so that most of the Gaussian width observed has to originate from inhomogeneous broadening. Some of the intensity of this resonance may be from a two-electron excitation to a bound state, which could be inhomogeneously broadened by vibrational excitations. Inhomogeneous broadening could also result from a slight offset of two or more overlapping resonances (e.g., one shape resonance state and one bound state or two shape resonance states). The t_{2g} resonance was observed, however, in the direct photoelectron spectrum of the sulfur $2p$ levels, indicating that the resonance must be at least partly a shape resonance [19]. If the observed line shape were determined mainly by two-electron excitations, then the shape resonance contribution would have an extraordinarily narrow linewidth (< 0.3 eV). The more likely possibility is that the line shape is partly or completely determined by the shape resonance.

The relatively large Lorentzian contribution to the line shape of the (S $2p_{3/2,1/2})^{-1}t_{2g}^1$ shape resonance is some-

what unexpected. The implication is that the vibrational effects upon this resonance differ from those of other known shape resonances. Shape resonances are generally believed to induce some vibrational excitation of the final-state core-ionized molecule [29]. Resulting photoabsorption line shapes should be inhomogeneously broadened. Ground-state vibrational (zero-point) motion may also couple to the transition, creating broad asymmetric line shapes [29]. The relatively small Gaussian contribution to the line shape indicates that both of these vibrational effects are small in the t_{2g} shape resonance. A study of the ionic fragmentation pattern obtained from the decay of this excited state also indicated that there is little vibrational excitation in this state [30].

The strong Lorentzian character of the line shape is consistent with a rapidly decaying quasibound shape resonance state, but is also consistent with an alternative interpretation of this feature as a resonance in more than one continuum channel. Core-hole lifetimes are generally longer than the lifetime of quasibound shape resonance states. This can be seen directly by comparing the narrow photoelectron peaks at resonance to the wide photoabsorption peaks [31]. The t_{2g} resonance may differ in that the mainly nonradiative decay of the core hole is faster than the departure of the quasibound electron. This could explain the large observed Lorentzian component of the line shape, but would also describe the t_{2g} peak not really as a shape resonance but rather as a quasibound one-electron excited state that decays rapidly by an Augerlike autoionization process. This would give the same final state as would a direct photoelectron transition from a subshell less tightly bound than sulfur $2p$. In general, this type of continuum-continuum coupling will be observed as a resonance in one photoelectron channel at the same photon energy as a shape resonance in another channel. Such an inter-channel resonance was observed in the valence photoelectron spectra of SF_6 and attributed to the t_{2g} shape resonance of the $1t_{2u}+5t_{1u}$ channel coupling to the $3e_g$ photoelectron channel [20]. This is not a normal shape resonance; the kinetic energy of the photoelectron is not tuned to the shape of the potential. The most general model of the $(\mathrm{S}\ 2p_{1/2,3/2})^{-1}t^1_{2g}$ resonance includes contributions from double excitations, a shape resonance, and continuum-continuum coupling. The results of the ionic fragmentation study [30] suggest that the direct shape resonance dominates. More work, is needed, however, for a complete understanding of the line shape.

The line-shape analysis also shows that the $(\mathrm{S}\ 2p_{1/2})^{-1}t^1_{2g}$ resonance, peak 4, is $\approx 13\%$ broader than the $(\mathrm{S}\ 2p_{3/2})^{-1}t^{-1}_{2g}$ resonance, peak 3. This is consistent with the above results for the widths of the $(\mathrm{S}\ 2p_{3/2,1/2})^{-1}a^1_{1g}$ resonances. Again it seems that the $(\mathrm{S}\ 2p_{1/2})^{-1}$ core hole decays faster than the $(\mathrm{S}\ 2p_{3/2})^{-1}$ core hole.

3. *Vibronic coupling*

Transitions to electronic final states which are not dipole allowed may still have noticeable intensity through vibronic coupling. If vibrational excitation occurs in non-totally-symmetric vibrational modes such that the final vibrational-electronic (vibronic) state is of a symmetry accessible by a dipole transition, the transition will occur, though usually with low intensity [32]. This phenomenon can explain two features of the spectra shown in Fig. 3. One feature is the three $(\mathrm{S}\ 2p_{3/2})^{-1}4p^1$ peaks E, F, and G mentioned in Sec. III. The other is the broad underlying intensity (shaded area in Fig. 3) in the photon-energy range 175–179 eV. This latter feature has been assigned to transitions into one or two inner-well orbitals with t_{1u} symmetry. Both features involve t_{1u} symmetry final-state orbitals. Direct excitation of these states is electric-dipole forbidden, but electric-quadrupole and magnetic-dipole allowed. Both features have more spectral weight in the EELS spectra than in the corresponding photoabsorption data [15]. This indicates that the higher-order transitions (electric quadrupole, magnetic dipole, etc.), which are induced by the EELS excitation process [33], enhance these two spectral features. They may only be observed in photoabsorption, where the dipole selection rule applies, if at least one quantum of a t_{1u} symmetry or t_{2u} symmetry vibrational mode is excited. There are two t_{1u} modes and one t_{2u} mode in SF_6.

This interpretation is further supported by the assignment of the remaining Rydberg structure given below. Attempts to assign peak E at 178.3 eV as a member of an s or d Rydberg series led to a poor description of the remaining peaks. As for the t_{1u} inner-well orbitals, they are known from theoretical work [34–36] and from previously measured EELS spectra at the fluorine K edge and the L_1 and K edges of sulfur [13,15]. Excellent spatial overlap with sulfur $2p$ electrons is expected, considering the intensity of the transition to the t_{1u} orbital below the sulfur L_1 edge [15].

The initially published spectra of the S $L_{2,3}$ region showed only the most intense features of the rich fine structure in the spectrum of Fig. 3. Several papers [18,35,37] assigned these weakly resolved peaks to transitions to $(\mathrm{S}\ 2p_{1/2,3/2})^{-1}t^1_{1u}$ states. The present work illustrates the success of the Rydberg formula in predicting the energies of these states. Their assignments as Rydberg states is further supported by their linewidths, which are much smaller than those of the $(\mathrm{S}\ 2p_{1/2,3/2})^{-1}$ inner-well resonances. The $(\mathrm{S}\ 2p_{1/2,3/2})^{-1}t^1_{1u}$ states anticipated by these early workers are observed here as the broad underlying intensity described above (shaded area in Fig. 3).

Vibronic coupling between the ground state and a dipole-forbidden electronic final state is actually mediated by one or more dipole-allowed excited electronic states. Such states mix with the dipole-forbidden electronic final state via vibronic interactions [32]. The mixing and thus the vibronically coupled transition are facilitated in this case by the presence of intense dipole-allowed transitions (the a_{1g}, t_{2g}, and e_g resonances) that are close in energy to the vibronically coupled states. Vibronic interaction between these sets of states is symmetry allowed through the two t_{1u} or one t_{2u} vibrational mode of SF_6. Trends of the t_{1u} vibrational-mode frequencies in series of halogen hexafluoride molecules suggest significant vibronic interaction between the a_{1g} and t_{1u} molecular orbitals [38].

B. Sulfur $L_{2,3}$ thresholds: Rydberg series

1. Rydberg formula

The energies of the Rydberg transitions in atoms are given by the Rydberg formula

$$E_{n,l} = V_{\text{ion}} - \mathcal{R}/(n-\delta_l)^2 , \quad (1)$$

where V_{ion} is the ionization potential of the subshell, $\mathcal{R}$ is the Rydberg constant, n and l are the principal and angular momentum quantum numbers of the Rydberg orbital, and δ_l is the quantum defect. The quantum defect depends on l because of the differing degrees of core penetration of s, p, d, etc. orbitals. δ_l will be largest for s orbitals, which have no centrifugal barrier, and will be close to zero for $l \geq 2$. This formula can sometimes successfully predict the energies of Rydberg states in molecules [39].

Dipole selection rules allow transitions to the s and d series Rydberg states below both the sulfur L_2 and L_3 edges, which are split by the spin-orbit interaction (see Sec. IV A 1). Basing the assignment on the sulfur atomic quantum numbers indicates that the s series should begin with $n=4$ and the d series with $n=3$. A least-squares fit of the spectrum of Fig. 3 was used to determine the best values for the quantum defects, vibrational spacings, and the energies of the absorption thresholds. Fit results for intensities and widths are most reliable for the more intense and well-isolated features. Derived values are also given for some of the weaker features, but they should not be regarded as definitive. The fit required the use of many adjustable parameters, and regions of overlapping peaks can probably be fitted nearly as well with other combinations of intensities and widths. The background was modeled by a linear contribution, the tail of two Voigt functions from peaks 3 and 4 (see Fig. 2), and several overlapping Gaussian peaks to represent the (S $2p_{1/2,3/2})^{-1}t_{1u}^1$ transitions. Two additional broad peaks (D and K) were necessary to obtain reasonable results. These may be viewed as essential modifications to the approximated line shape of the (S $2p_{1/2,3/2})^{-1}t_{1u}^1$ resonances.

The results of the least-squares fit are shown in Fig. 3 and in Table II. The peak assignments agree with those of previous reports based on spectra with fewer discernible features [12,15]. Even the previously unobserved features are easily assigned [e.g., peak a, the shoulder at 180.7 eV, is the (S $2p_{1/2})^{-1}6s^1$ state]. A single value of the quantum defect is sufficient for each series beyond the lowest-energy peak. The energy of the (S $2p_{3/2})^{-1}4s^1$ state (peak A) is perturbed by -37 meV and that of the (S $2p_{1/2})^{-1}4s^1$ state (peak H) is perturbed by -35 meV from the prediction based on this quantum defect. The perturbations of the (S $2p_{1/2,3/2})^{-1}3d$ states are discussed below (see Sec. IV B 2). The values of the quantum defect obtained, $\delta_s = 1.80$ and $\delta_d = -0.03$, follow the predictions of the simple penetration model mentioned above. The success of the Rydberg formula suggests that the states are quite atomiclike regarding penetration of the screening electrons by the excited electron. Such simplicity in a polyatomic molecule, with 70 electrons, may be a result of the small size of the molecule; the ground-state S—F bond length is only 1.561 Å, while the smallest Rydberg orbital, 4s, has a mean radius of ≈ 3.8 Å, assuming the quantum defect given above. This shows that even the lowest Rydberg orbital lies mainly in the outer well of Fig. 1. Further evidence for the extra-molecular nature of these Rydberg states comes from a recent photoabsorption experiment [14]. That work showed that the sulfur $L_{2,3}$ Rydberg resonances observed, as here, for gas-phase SF_6 are absent in the corresponding spectrum of condensed SF_6.

2. Multiplet splitting

The octahedral symmetry of the SF_6 molecule induces multiplet splitting of each sulfur atomic d orbital into t_{2g} and e_g molecular orbitals. Core-excited Rydberg states show multiplet splitting in many molecular systems [4–6,40]. Generally, this splitting is expected to be largest for the lowest states of a given Rydberg series because these states feel the strongest anisotropic molecular field. In the d-symmetry Rydberg series observed here, multiplet splitting is resolved only for the (S $2p_{1/2,3/2})^{-1}3d^1$ states. Fits of the line shape near the expected energy of the (S $2p_{3/2})^{-1}3d^1$ state reveal the presence of two shoulders at 178.80 and 178.85 eV just above the peak at 178.76. The most likely assignment is that the peak at 178.76 is the (S $2p_{3/2})^{-1}3d$-t_{2g}^1 state, the first shoulder is the (S $2p_{3/2})^{-1}3d-e_g^1$ state, and the higher shoulder is a vibrational sideband associated with the (S $2p_{3/2})^{-1}3d-t_{2g}^1$ state. This results in a multiplet splitting of 40 meV and a vibrational spacing of 84 meV. The weighted average of the energies of the (S $2p_{3/2})^{-1}3d$-t_{2g}^1 and -e_g^1 states is perturbed by -24 meV from the prediction based on the quantum defect given above.

Analysis of the line shape around the expected energy of the (S $2p_{1/2})^{-1}3d^1$ state is complicated by the overlapping Rydberg states leading up to sulfur L_3 edge at 180.27 eV. The fit shows, however, that there is more intensity in the region 179.95–180.05 eV than would be expected from only the (S $2p_{3/2})^{-1}7d^1$ state at 180.00 eV. This result is consistent with the presence of the (S $2p_{1/2})^{-1}3d$-e_g^1 state at 180.00 eV, 40 meV above the (S $2p_{1/2})^{-1}3d$-t_{2g}^1 state at 179.96 eV. Similarly, the vibrational shoulder expected for the (S $2p_{1/2})^{-1}3d$-t_{2g}^1 state overlaps the (S $2p_{3/2})^{-1}8d^1$ state, accounting for its anomalously high intensity. The energy of the (S $2p_{1/2})^{-1}3d$-t_{2g}^1 state is perturbed by -36 meV from the prediction based on the quantum defect given above.

3. Linewidths of the Rydberg resonances

The linewidths of the Rydberg resonances are significantly smaller than those of the inner-well resonances near the sulfur $L_{2,3}$ thresholds, as can be seen by comparing the values given in Tables I and II. Exact linewidths for the individual Rydberg states are not easily obtained because nearly all the resonances lie in regions of overlapping features. Nevertheless, the fit is good enough in most regions to allow the deconvolution of reli-

able individual linewidths for the more intense resonances. In particular, the extracted total linewidths (FWHM) of the (S $2p_{3/2})^{-1}3d$-t_{2g}^1, (S $2p_{3/2})^{-1}5s^1$, and (S $2p_{3/2})^{-1}4d^1$ states (peaks *J*, *L*, and *O*) are 57, 54, and 60 meV, respectively. Assuming a Gaussian contribution of 40 meV from the instrumental resolution, the derived Lorentzian natural linewidths are 28, 24, and 32 meV, respectively. These results are striking, considering the much larger Lorentzian width (at least 220 meV) of the energetically nearby inner-well (S $2p_{1/2,3/2})^{-1}a_{1g}^1$ states (see Sec. IV A 2).

The large difference in the natural linewidths of the Rydberg resonances and the (S $2p_{1/2,3/2})^{-1}a_{1g}^1$ resonances can be explained by considering the decay mechanisms of these states. Semiempirical calculations [41] for atomic sulfur show that a sulfur $2p$ core hole will decay primarily by an Auger process. The predicted natural linewidth is 54 meV. In the case of SF_6, the fluorine atoms withdraw electron density from the region of the sulfur core hole [42], resulting in a decrease in the Auger decay rate simply because the valence electrons are further away than in the atom. This qualitatively explains the natural linewidth of <54 meV for some of the Rydberg resonances observed in the present work, and also predicts a very narrow linewidth for photoelectrons emitted from the sulfur $2p$ subshell in SF_6. In the (S $2p_{1/2,3/2})^{-1}a_{1g}^1$ resonances, the excited electron occupies an orbital which must overlap the S $2p$ core hole strongly, since the absorption resonance is intense. The availability of another electron for Auger decay significantly accelerates the process, resulting in the large natural linewidths observed for these states. This phenomenon emphasizes the substantial difference between the spatial distributions of the inner-well a_{1g} orbital and the outer-well Rydberg orbitals. Moving a single electron from the inner well to the outer well can increase the lifetime of a core-excited state by as much as one order of magnitude.

4. *Vibrational structure*

Several of the *s*- and *d*-symmetry Rydberg states observed show high-energy shoulders. These may be assigned to final states which include the excitation of a quantum of vibrational energy. The only dipole-allowed vibrational excitation is for the single a_{1g} symmetric stretch mode (ν_1). This rule applies to all the *s*- and *d*-symmetry excitations. The best example is the (S $2p_{3/2})^{-1}4s^1$ state (peak *A*) at 177.42 eV and its shoulder at 177.50 eV (peak *B*). This shoulder is assigned to the vibrational excitation of the a_{1g} mode in the (S $2p_{3/2})^{-1}4s^1$ state. A Franck-Condon analysis [28] of the (S $2p_{3/2})^{-1}4s^1$ peak manifold (see Fig. 6) used harmonic-oscillator potentials and Voigt line shapes. The excited-state parameters obtained were $h\nu_e=69$ meV (557 cm^{-1}) and $R_e=1.58$ Å (or 1.54 Å) compared to $h\nu_g=95.9$ meV (774 cm^{-1}) and $R_g=1.561$ Å in the ground state [26,27]. As noted above (in Sec. IV A 2), in the harmonic-oscillator approximation used here, equal contractions and extensions of the bond give equivalent results, so the fit cannot distinguish between the two values given for the S—F bond length R_e. However, the decrease in the vibrational energy spacing suggests a weakening of the S—F bonds, corresponding to a lengthening of the bond distance. The relative Franck-Condon factors resulting from the fit are 1.000:0.417:0.032:0.000.

The (S $2p_{1/2})^{-1}4s^1$ state, peak *H* at 178.63, has the shoulder *I* at 178.69. This shoulder is a vibrational excitation analogous to peak *B*. A Franck-Condon fit is not practical in this region of overlapping peaks, but the vibrational spacing determined from the least-squares fit of Fig. 3 is 61 meV, which is close to the value determined for the (S $2p_{3/2})^{-1}4s^1$ state. The derived intensity ratio of peak *I* to peak *H* is 1.00:0.417, identical to the corresponding value for the (S $2p_{3/2})^{-1}4s^1$ state. The similarity of the vibrational parameters of these two states is expected, because the difference in the core hole, (S $2p_{3/2})^{-1}$ vs (S $2p_{1/2})^{-1}$, should have little influence on the inter-atomic bonds.

The (S $2p_{3/2})^{-1}5s^1$ peak *L* is 178.95 eV shows a vibrational shoulder *M* at 179.02 eV. The small intensity ratio estimated from the fit (1.00:0.13) indicates that the bond length of the (S $2p_{3/2})^{-1}5s^1$ state changes less relative to the ground state than that of the (S $2p_{3/2})^{-1}4s^1$ state. Similarly, the spacing determined from the fit, 74 meV, is closer to the ground-state value than the spacing determined above for the (S $2p_{3/2})^{-1}4s^1$ state. These results and the lack of detectable vibrational structure in the higher members of this series are expected, because higher Rydberg orbitals have less amplitude within the molecule and are more completely nonbonding. The (S $2p_{1/2})^{-1}5s^1$ peak *V* at 180.15 eV shows a vibrational shoulder *W* at 180.22 eV. This feature has not been fit very accurately because it lies in a region where the background is difficult to model.

Vibrational excitations are also observed in several of the *d*-symmetry Rydberg states. The (S $2p_{3/2})^{-1}3d$-t_{2g}^1 state, as mentioned in Sec. IV B 2, has a vibrational sideband with a spacing of 85 meV and an intensity ratio of 1.00:0.12. This ratio is comparable to that of the nearby (S $2p_{3/2})^{-1}5s^1$ state, while the spacing is slightly larger, indicating that the $3d$-t_{2g} orbital is slightly more nonbonding than the $5s$ orbital. These parameters cannot be derived for the (S $2p_{1/2})^{-1}3d$-t_{2g}^1 state, where a vibrational shoulder may be present, but is obscured by the overlapping (S $2p_{3/2})^{-1}8d^1$ state. The (S $2p_{3/2})^{-1}4d^1$ state, peak *O* at 179.44 eV, shows a weak vibrational shoulder *P* at 179.54 eV. The corresponding (S $2p_{1/2})^{-1}4d^1$ state, peak *Z* at 180.64 eV, does not show a vibrational shoulder. Peak *P* might therefore be alternatively assigned as a second vibrational peak of the (S $2p_{1/2})^{-1}4p^1$ state, peak *N* at 179.36. The (S $2p_{3/2})^{-1}5d^1$ peak *Q* at 179.74 eV has a vibrational shoulder *R* at 179.83 eV, and the corresponding (S $2p_{1/2})^{-1}5d^1$ peak *b* at 180.94 eV has a similar shoulder *c* at 181.03 eV. Both of these vibrational excitations have a spacing of $\approx$95 meV, which is close to the ground-state value (95.9 meV). This reflects the nonbonding nature of these higher Rydberg states.

5. *Sulfur p Rydberg orbitals*

Peak E at 178.23 eV has been assigned to the (S $2p_{3/2})^{-1}4p^1$ state for reasons discussed above (see Sec. IV A 3). In this assignment, this state sits atop a relatively intense, though broad, (S $2p_{1/2})^{-1}\,t_{1u}^1$ peak centered at ≈ 177.5 eV. These excited states share the same symmetry and similar energies, so nonvibronic mixing is likely to occur. Essentially, the (S $2p_{3/2})^{-1}4p^1$ state acquires some inner-well character from this mixing. In contrast, the (S $2p_{1/2})^{-1}4p^1$ state will not be perturbed as strongly by the (S $2p_{1/2})^{-1}t_{1u}^1$ state(s) because the energy separation is larger. This may be seen directly in Fig. 5, where the (S $2p_{3/2})^{-1}4p^1$ state overlaps the (S $2p_{1/2})^{-1}t_{1u}^1$ shaded region, while the (S $2p_{1/2})^{-1}4p^1$ state is ≈ 1.0 eV above the top of this region. To facilitate this comparison, the spin-orbit splitting of the (S $2p_{1/2,3/2})^{-1}t_{1u}^1$ resonances is shown in the figure, although it was not resolved in the spectra. The (S $2p_{3/2})^{-1}4p^1$ state may be shifted to a higher energy by the interaction with the (S $2p_{1/2})^{-1}t_{1u}^1$ state(s), reducing the observed spin-orbit splitting of the (S $2p_{1/2,3/2})^{-1}4p^1$ pair. The (S $2p_{1/2})^{-1}4p^1$ state can thus be assigned to the weak feature K at 179.3 eV. This assumes a shift of ≈ 0.1 eV of the (S $2p_{3/2})^{-1}4p^1$ state to higher energy. This is a tentative assignment, but it is the most plausible one. Peaks X and Y at 180.42 and 180.50 eV have been assigned to the (S $2p_{1/2})^{-1}5p^1$ state and a vibrational sideband, respectively. These are very weak resonances, and their assignment is not certain. A corresponding (S $2p_{3/2})^{-1}5p^1$ state may be present at 179.22 eV, but only barely above the noise level.

Note that the vibronically coupled (S $2p_{3/2})^{-1}4p^1$ transition (peak E) must already include the excitation of at least one quantum of an antisymmetric vibrational mode of the excited state. Assuming the offset of the transition energy to be 76.2 meV, the corresponding quantum defect derived from the energy of peak E is $\delta_p = 1.48$. This value is not unique; it depends on the vibrational offset, which was rather arbitrarily chosen here to equal the energy spacing of the ground-state ν_4 mode (t_{1u} symmetry). Use of the ground-state energies [27] of the other two antisymmetric modes, ν_3 (117.5 meV, t_{1u} symmetry) and ν_6 (42.9 meV, t_{2u} symmetry), would result in $\delta_p = 1.50$ and 1.46, respectively. This analysis assumes that the Jahn-Teller effect is small for this electronic state. If the Jahn-Teller effect is large, which is possible, the offset of peak E from the ground vibrational state of the (S $2p_{3/2})^{-1}4p^1$ electronic state will also reflect the Jahn-Teller splitting of the vibrational states.

Peak E shows two shoulders F and G at higher energies. These are assigned to transitions to (S $2p_{3/2})^{-1}4p^1$ states with additional vibrational excitation. The spacings of the shoulders from the main line determined from a least-squares fit are 116 and 220 meV. As in the case of the (S $2p_{3/2})^{-1}4s^1$ state, excitation of the a_{1g} vibrational mode is allowed. Vibrational excitations are also allowed of any combination of antisymmetric modes with an odd number of total quanta, e.g., $2\nu_3 + 1\nu_4$. This odd number includes the single quantum of an antisymmetric vibration which contributes to the energy of peak E. If the Jahn-Teller effect is small in this electronic state, a_{1g} vibrational excitations should dominate. The ground-state energy of this vibration ($h\nu_g = 96$ meV) is roughly comparable to the spacings observed for peaks F and G. If the Jahn-Teller effect is large, excitation of the antisymmetric modes may have significant intensity. Each combination of the antisymmetric vibrational modes will be split into multiple components by the dynamic Jahn-Teller effect. The complexity of the resulting situation makes any assignment of these vibrational excitations highly speculative.

6. *Energies of the sulfur $L_{2,3}$ thresholds*

The energies of the sulfur $L_{2,3}$ thresholds are determined by fitting the Rydberg series. The resulting values, given in Table II, are in agreement with previous results from photoabsorption, EELS, and photoelectron spectroscopy [8–12, 15,21,22], within the expected accuracy of monochromator calibration. The absolute energies from EELS are probably more accurate than those given here. The fit confirms what is apparent by visual inspection; there is no measurable edge jump at these thresholds. This is actually expected for systems with intense resonances near threshold [43]. The intense t_{2g} absorption lines just above the thresholds, as well as the other intense absorption features close by, "borrow" oscillator strength from the background of direct photoexcitation of sulfur $2p$ electrons into low kinetic-energy states of the continuum.

C. Sulfur $L_{2,3}$ thresholds: Comparison with theory

There are four main theoretical papers concerning the core-level photoabsorption of SF_6. Gianturco, Guidotti, and Lamanna (GGL) used a linear combination of atomic orbitals-molecular orbital LCAO-MO approach [35]. Hay used the improved-virtual-orbital (Hartree-Fock) method [44]. Wallace employed the multiple-scattering $X\alpha$ method [36]. Nakamatsu, Mukoyama, and Adachi (NMA) used the discrete variational $X\alpha$ method [34]. Overall, the theoretical results give a fairly good qualitative agreement with experiment. The assignments given in this paper are essentially consistent with these theoretical results, with the following notable results and exceptions: (1) Wallace predicts both the s and the d Rydberg series below the sulfur $L_{2,3}$ edges. The calculated multiplet splitting of the $3d$ state into t_{2g} and e_g species is ≈ 100 meV, in agreement with the result of Hay, and much less for higher nd states. The observed splitting was 40 meV (see Sec. IV B 2). (2) NMA describe the resonances at 182–186 eV as transitions to two overlapping (S $2p_{1/2,3/2})^{-1}t_{2g}^1$ doublets rather than to one doublet. Likewise, the resonance at 196 eV is attributed to two (S $2p_{1/2,3/2})^{-1}e_g^1$ doublets rather than to one doublet. (3) The results of NMA suggest that the potential-barrier model shown in Fig. 1 is not accurate for SF_6. The description of excited states as inner- and outer-well states remains useful, however, to specify the spatial distribution of the excited electron (see Sec. I). (4) Hay cal-

culated orbital energies for the (S $2p$)$^{-1}4s^1$, $5s^1$, $4p^1$, and $3d^1$ states that agree closely with those observed. His predictions for the (S $2p$)$^{-1}a_{1g}^1$ and (S $2p$)$^{-1}t_{1u}^1$ states are not as accurate. The results in his paper indicate that the (S $2p$)$^{-1}t_{1u}^1$ state observed here (shaded region in Fig. 3) is a Rydberg state when it is excited at the more weakly bound thresholds (i.e., valence and subvalence). The state shifts to a larger orbital energy (further below the edge) in the core-hole states. This transition from Rydberg to valence character occurs as the orbital "collapses" into the deepening inner well (see Fig. 1). This is reflected by an approximate change of $+1$ in the quantum defect, or, equivalently, a change in the number of the Rydberg states (i.e., $5p$ is relabeled $4p$, etc.). The latter representation is used in the present assignment, which labels peak D as the $4p$ state. Hay refers to the same resonance as the $5p$ state.

D. Fluorine K threshold

Previous reports [13,15] of XANES spectra at the fluorine K edge of SF_6 have given assignments similar to those in Table III and Sec. III. The assignments here differ only in the region from 692 to 698 eV (see Fig. 4). The spectrum clearly shows one peak 10 at 694.7 eV with a low-energy shoulder 9 at 692.9 eV. Careful line-shape analysis of the spectrum in Fig. 4, using a Gaussian-broadened arctangent function to model the edge jump, revealed additional intensity in this range (peak 10). The results of the fit are shown in Fig. 4 and Table III. Based on the theoretical results discussed below, the two peaks 9 and 10 are assigned primarily to two (F $1s$)$^{-1}t_{1u}^1$ final states. The additional peak 11 at $\approx$697 eV has been tentatively assigned to a manifold of weaker (F $1s$)$^{-1}t_{1u}^1$ final states; but below-edge contributions from s, p, and d Rydberg states cannot be excluded. A previous report [15] suggested that the $\approx$1.8 eV splitting of the 694.7-eV peak (into peaks 9 and 10) might be the result of initial-state symmetry splitting of the fluorine $1s$ core level. This is unlikely, since no splitting of this level was observed in core-level photoelectron spectra taken with a resolution of $\approx$0.8 eV [45].

The least-squares fit of the line shape showed large Gaussian contributions to all peaks, indicating inhomogeneous broadening. No vibrational structure could be detected at a resolution as low as $\approx$310 meV. The line shape of the (F $1s$)$^{-1}t_{2g}^1$ shape resonance, in contrast to the corresponding resonance at the $L_{2,3}$ thresholds, does not have a large Lorentzian contribution. This inhomogeneous broadening could be explained by the stronger vibrational excitations expected in a core-excited state with reduced symmetry, as in F-core-excited SF_6. An alternative explanation is suggested below.

The four main theoretical papers cited above (in Sec. III C) are also qualitatively successful in the assignment of the fluorine K threshold region, with the following notable results and exceptions. GGL and NMA predict only one strong transition to a t_{1u} orbital below the fluorine K threshold. Neither work predicts a resonance of any symmetry to correspond to shoulder 9 at 692.9 eV. NMA also predict two weaker (F $1s$)$^{-1}t_{1u}^1$ resonances in the region where extra intensity was observed in this study. Wallace predicts three or four strong and several weak (F $1s$)$^{-1}t_{1u}^1$ resonances in the pre-edge region. GGL assign the resonance just above the fluorine K edge to a transition to a t_{1u} orbital rather than a t_{2g} orbital. NMA assign approximately one third of the intensity of this resonance to a (F $1s$)$^{-1}t_{1u}^1$ state and the remaining intensity to a slightly lower (F $1s$)$^{-1}t_{1g}^1$ state. This is another possible explanation for the difference in line shapes observed between the (S $2p_{1/2,3/2}$)$^{-1}t_{2g}^1$ and the (F $1s$)$^{-1}t_{2g}^1$ states; the resonance above the fluorine K edge may be inhomogeneously broadened by the presence of an offset (F $1s$)$^{-1}t_{1u}^1$ contribution with possibly a non-Lorentzian line shape. Hay again had success in predicting the orbital energies of some states below threshold. His results agree very well with the present assignment, with the added possibilities that (1) peak 9 includes contributions from a (F $1s$)$^{-1}a_{1g}^1$ state and (2) peak 10 includes contributions from (F $1s$)$^{-1}a_{1g}^1$, (F $1s$)$^{-1}e_g^1$, or (F $1s$)$^{-1}t_{2g}^1$ states. Overall, the results of Wallace and Hay are in good agreement with the present experimental measurements. Since Hay's work did not predict relative intensities of transitions, Wallace's results were in fact the main guide for the present assignments.

ACKNOWLEDGMENTS

Expert assistance by the staff of BESSY is acknowledged. D. A. S. thanks the Alexander-von-Humboldt foundation for support. This work was supported by the Director, Office of Energy Research, Office of Basic Energy Sciences, Chemical Sciences Division of the U.S. Department of Energy under Contract No. DE-AC03-76SF00098 and the Bundesminister für Forschung and Technologie, Project No. 05-KEAXI 3/TP03.

*Present address: Pennsylvania State University, 114 Kern Graduate Building, University Park, PA 16802.

[1] M. Domke, T. Mandel, A. Puschmann, C. Xue, D. A. Shirley, G. Kaindl, H. Petersen, and P. Kuske, Rev. Sci. Instrum. **63**, 80 (1992).

[2] M. Domke, A. Puschmann, C. Xue, D. A. Shirley, G. Kaindl, and H. Petersen, Synchrotron Radiat. News **3**, No. 5, 15 (1990).

[3] P. A. Heimann, F. Senf, W. McKinney, M. Howells, R. D. van Zee, L. J. Medhurst, T. Lauritzen, J. Chin, J. Meneghetti, W. Gath, H. Hogrefe, and D. A. Shirley, Phys. Scr. **T31**, 127 (1990).

[4] C. T. Chen, Y. Ma, and F. Sette, Phys. Rev. A **40**, 6737 (1989).

[5] Y. Ma, C. T. Chen, G. Meigs, K. Randall, and F. Sette, Phys. Rev. A **44**, 1848 (1991).

[6] M. Domke, C. Xue, A. Puschmann, T. Mandel, E. Hudson, D. A. Shirley, and G. Kaindl, Chem. Phys. Lett. **173**, 122 (1990); **174**, 68 (1990).

[7] For a review see G. C. King and F. H. Read, in *Atomic*

Inner-Shell Physics, edited by B. Crasemann (Plenum, New York, 1985), pp. 317–375.
[8] T. M. Zimkina and V. A. Fomichev, Dokl. Akad. Nauk SSSR **169**, 1304 (1966) [Sov. Phys. Dokl. **11**, 726 (1967)]; A. S. Vinogradov and T. M. Zimkina, Opt. Spektrosk. **32**, 33 (1972) [Opt. Spectrosc. USSR **31**, 364 (1971)].
[9] M. Nanamura, Y. Morioka, T. Hayaishi, E. Ishigura, and M. Sasanuma, in *III International Conference on Vacuum Ultraviolet Radiation Physics: Conference Digest,* edited by Y. Nakai (Physical Society of Japan, Tokyo, 1971), pp. A1–6.
[10] D. Blechschmidt, R. Haensel, E. E. Koch, U. Nielsen, and T. Sagawa, Chem. Phys. Lett. **14**, 33 (1972).
[11] B. M. Addison, K. H. Tan, G. M. Bancroft, and F. Cerrina, Chem. Phys. Lett. **129**, 468 (1986).
[12] E. S. Gluskin, A. A. Krasnoperova, and L. N. Mazalov, Zh. Strukt. Khim. **18**, 185 (1977) [J. Struct. Chem. USSR **18**, 156 (1977)].
[13] T. M. Zimkina and A. S. Vinogradov, J. Phys. (Paris) Colloq. **C4**, 3 (1971); R. E. LaVilla, J. Chem. Phys. **57**, 899 (1972).
[14] J. S. Tse and Z. F. Liu, Phys. Rev. A **44**, 7838 (1991).
[15] A. P. Hitchcock and C. E. Brion, Chem. Phys. **33**, 55 (1978).
[16] H. Petersen, Opt. Commun. **40**, 402 (1982); H. Petersen, Nucl. Instrum. Methods A **246**, 260 (1986).
[17] J. L. Dehmer, J. Chem. Phys. **56**, 4496 (1972).
[18] W. H. E. Schwarz, Angew. Chem. Int. Ed. Engl. **13**, 454 (1974); V. I. Nefedov, Zh. Strukt. Khim. **11**, 292 (1970); [J. Struct. Chem. USSR **11**, 272 (1970)].
[19] T. A. Ferrett, D. W. Lindle, P. A. Heimann, M. N. Piancastelli, P. H. Kobrin, H. G. Kerkhoff, U. Becker, W. D. Brewer, and D. A. Shirley, J. Chem. Phys. **89**, 4726 (1988).
[20] J. L. Dehmer, A. C. Parr, S. Wallace, and D. Dill, Phys. Rev. A **26**, 3283 (1982).
[21] K. Siegbahn, C. Nordling, G. Johansson, J. Hedman, P. F. Hedén, K. Hamrin, U. Gelius, and T. Bergmark, *ESCA Applied to Free Molecules* (North-Holland, Amsterdam, 1969), pp. 94–98.
[22] U. Gelius, J. Electron Spectrosc. Relat. Phenom. **5**, 985 (1974).
[23] R. V. Vedrinskii, A. P. Kovtun, V. V. Kolesnikov, Y. F. Migal, E. V. Polozhentsev, and V. P. Sachenko, Izv. Akad. Nauk SSSR Ser. Fiz. **38**, 434 (1974); [Bull. Acad. Sci. USSR Ser. Phys. **38**, 8 (1974)].
[24] U. Nielson, R. Haensel, and W. H. E. Schwarz, J. Chem. Phys. **61**, 3581 (1974).
[25] A. R. Boate, J. R. Morton, and K. F. Preston, J. Phys. Chem. **80**, 2954 (1976).
[26] L. S. Bartell and S. K. Doun, J. Mol. Struct. **43**, 245 (1978); V. C. Ewing and L. E. Sutton, Trans. Faraday Soc. **59**, 1241 (1963).
[27] Y. M. Bosworth, R. J. H. Clark, and D. M. Rippon, J. Mol. Spectrosc. **46**, 240 (1973); R. S. McDowell, J. P. Aldridge, and R. F. Holland, J. Phys. Chem. **80**, 1203 (1976).
[28] E. Hutchisson, Phys. Rev. **36**, 410 (1930).
[29] J. L. Dehmer, A. C. Parr, and S. H. Southworth, in *Handbook on Synchrotron Radiation,* edited by G. V. Marr (North-Holland, Amsterdam, 1987), Vol. II, pp. 280–284.
[30] A. P. Hitchcock, C. E. Brion, and M. J. Van der Wiel, J. Phys. B **11**, 3245 (1978).
[31] C. M. Truesdale, D. W. Lindle, P. H. Kobrin, U. E. Becker, H. G. Kerkhoff, P. A. Heimann, T. A. Ferrett, and D. A. Shirley, J. Chem. Phys. **80**, 2319 (1984).
[32] G. Herzberg, *Molecular Spectra and Molecular Structure* (Van Nostrand Reinhold, New York, 1966), Vol. III, pp. 137–41.
[33] G. C. King and F. H. Read, in *Atomic Inner-Shell Physics* (Ref. [7]), pp. 357–365.
[34] H. Nakamatsu, T. Mukoyama, and H. Adachi, J. Chem. Phys. **95**, 3167 (1991); Chem. Phys. **143**, 221 (1990).
[35] F. A Gianturco, C. Guidotti, and U. Lamanna, J. Chem. Phys. **57**, 840 (1972).
[36] R. Scott Wallace, Ph.D. thesis, Boston University, 1980.
[37] V. I. Nefedov and V. A. Fomichev, Zh. Strukt, Khim. **9**, 279 (1968) [J. Struct. Chem. USSR **9**, 217 (1968)].
[38] A. R. Boate, J. R. Morton, K. F. Preston, and S. J. Strach, J. Chem. Phys. **71**, 388 (1979).
[39] G. Herzberg, *Molecular Spectra and Molecular Structure* (Ref. [32]), pp. 340–341.
[40] G. R. Wright and C. E. Brion, J. Electron Spectrosc. Relat. Phenom. **4**, 25 (1974).
[41] M. O. Krause and J. H. Oliver, J. Phys. Chem. Ref. Data **8**, 329 (1979).
[42] D. P. Santry and G. A. Segal, J. Chem. Phys. **47**, 158 (1967); G. L. Bendazzolli, P. Palmieri, B. Cadioli, and U. Pincelli, Mol. Phys. **19**, 865 (1970); P. Jeffrey Hay, J. Am. Chem. Soc. **99**, 1003 (1977).
[43] U. Fano and J. W. Cooper, Rev. Mod. Phys. **40**, 441 (1968).
[44] P. Jeffrey Hay, J. Am. Chem. Soc. **99**, 1013 (1977).
[45] K. Siegbahn, C. Nordling, G. Johansson, J. Hedman, P. F. Hedén, K. Hamrin, U. Gelius, and T. Bergmark, *ESCA Applied to Free Molecules* (Ref. [21]), p. 24.